Received: July 30, 2023. Revised: September 6, 2023. 458

International Journal of
Intelligent Engineering & Systems

http://www.inass.org/

Lung Nodule Segmentation Using Cat Swarm Optimization Based Recurrent Neural Network

Spoorthi Basavarajappa[1]* **Shanthi Mahesh[1]**

[1]*Department of Information Science and Engineering, Atria Institute Technology, Bengaluru, India*
* Corresponding author's Email: spoorthi.kala@gmail.com

Abstract: Nodule segmentation in lung computed tomography (CT) images is a significant part of the detection and diagnosis of lung cancer. Automatic analysis of lung CT images is necessary to calculate lung nodule characteristics for recognizing malignancy. In recent years, deep learning and neural networks have been used in medical applications. Deep learning utilizes neural networks to train huge amounts of information which effectively learns the nodule features in lower to higher grades for segmenting and predicting the medical images. In this paper, the proposed cat swarm optimization (CSO) based recurrent neural network (RNN) is utilized for lung nodule segmentation. The proposed model is estimated on the freely accessible lung image database consortium and image database resource initiative (LIDC-IDRI) dataset. The proposed model is segmented by using the markov random field (MRF) based firefly algorithm (FA) and cuckoo search algorithm (CSA). The result shows that the proposed CSO based RNN model delivers performance metrics like dice coefficient (DC) loss and accuracy values of about 96.28% and 90.28% respectively, which ensures accurate nodule segmentation in lung CT images.

Keywords: Cat swarm optimization, Computed tomography images, Medical diagnosis, Nodule segmentation, Recurrent neural network.

1. Introduction

Nodule segmentation in lung CT images plays a significant role in the clinical diagnosis of lung tumors. Among the nodule variety, the solitary nodule has simple segmentation and clear boundaries while the non-solitary nodule has unclear boundaries [1]. For instance, the volume doubling time (VDT) and mass doubling time (MDT) are evaluated based on nodule segmentation which is an important part of lung nodule treatment and diagnosis [2]. In medicine, nodules lesser than 10mm in diameter are managed by CT to decide whether is malignant tumor [3]. Nodules expand in a short range (VDT<20) for long range (VDT500) are most likely benign and these benign nodules are managed by medicines only [4]. The nodules with the VDT (between 30-500) are most probably too malignant and need operative treatment [5]. The calculation of both VDT and MDT needs the exact and compatible nodule segmentation more than two times and the output is critical [6]. To handle these types of problems, it is essential to establish computer-aided or automatic lung nodule segmentation [7].

The perfect segmentation of the lung nodules is difficult, by considering nodule location, shape, size, and texture and the intensity may vary with the boundaries [8]. There are several kinds of lung nodules such as juxta vascular, isolated, juxta pleural, cavitary, calcific, ground-glass opacity, and small nodules [9]. Automatic investigation of lung CT images is necessary to calculate lung nodule characteristics to recognize malignancy [10]. The lung nodule segmentation determines the malignancy by investigating the nodule size and structure [11]. Other nodule segmentations have been represented in previous years and their accuracy is not high because of various challenges in lung nodule segmentation [12]. In recent years, deep learning and neural networks have been used in CT images for medical applications. Deep learning utilizes neural networks to train huge amounts of information, effectively

learn the nodule features in lower grades and form higher-grade features to segment and predict the medical images [13]. The contribution of this proposed paper is specified as follows:

- The min-max normalization technique is employed to pre-process the data. The firefly algorithm and cuckoo search algorithm are used for segmentation.
- The shape and texture-based feature extraction is utilized for generating more informative data.
- A cat swarm optimization (CSO) based recurrent neural network (RNN) model is introduced using the LIDC-IDRI dataset for nodule segmentation in lung CT images.

The rest of the portion present in the manuscript is organized as follows: Section 2 illustrates the literature review. The block diagram of the proposed model is presented in section 3. The experimental result of this proposed model is illustrated in section 4. Section 5 describes the summary of this paper.

2. Literature survey

Zhang [14] introduced a multiscale dense residual neural network based lung nodule segmentation in CT images using LIDC-IDRI dataset. The dense residual network connection and the convolution design of the expanded sawtooth were attached in the feature extraction. Additionally, the local residual design was added to the unsampling process. This MDRU-net model accurately makes the segmentation outputs and it can reuse the image multiscale features. However, the limitations such as low nodule tissues into foreground areas with false positives and unsatisfactory segmentation effects.

Usman and Shin [15] developed a lung nodule segmentation for a dual encoder based hard attention network with an adaptive ROI mechanism using LIDC-IDRI dataset. This proposed model was used for producing the 3-dimensional segmentation of lung nodules with the basic vision. This model was used to minimize the computational complexity by optimizing the performance in terms of execution duration. This developed model has an enormous increase in the computational cost which hinders the solutions in real-time clinical applications.

Banu [16] implemented a lung nodule segmentation for attention- aware weight excitation U-Net (AWEU-Net) using LIDC-IDRI and LUNA16 datasets. The PAWE and CAWE model was used for connection among the channel and spatial features. The CNN model was used to learn important attributes to improve the capability among non-nodule and nodule features. This developed model with the deep segmentation network is better, to reduce small object boundaries. However, it has an high computational cost and this model relies on various preprocessing and postprocessing procedures.

Shi [17] introduced an automatic lung nodule segmentation for aggregation U-Net generative adversarial networks (AUGAN) using LIDC-IDRI dataset. The GAN was developed for performing the image segmentation and the AUGAN was developed for automatic segment nodules in lung CT images. This proposed model does not rely on any kind assumptions while a huge number of standard methods assume that the data accept some specific distribution. The proposed model produces restricted sample varieties and highly sensitive to the hyperparameter selections.

Singadkar [18] developed a lung nodule segmentation based on a deep deconvolutional residual network (DDRN) for CT images using the LIDC-IDRI dataset. This proposed model was trained and captured several varieties of nodules from two-dimensional CT images. This model uses short and long connections in convolutional and deconvolutional networks to maintain the spatial details and it helps to increase convergence of the deep networks. However, this developed model nodule segmentation with a fixed size of morphological operator is difficult.

Inayatul Haq [19] presented a machine learning technique for lung nodule segmentation and classification from CT scan in LIDC-IDRI dataset. The developed model easily recognizes the nodule by comparing multiple CT images. The CNN technique is employed to classify the lung nodule effectively which includes five classes. This model provides a radiologist additional information to work with diagnosing nodule in earlier stages. The developed model achieves high accuracy and capable to detect the false positive rate. However, this developed model has high computational time with highly sensitive rate.

Imran Nazir [20] suggested an effective segmentation and classification for lung nodule detection using merged CT images in LIDC-IDRI dataset. The image fusion methodology is utilized over laplacian pyramid (LP) decomposition with adaptive sparse representation (ASR). The developed method integrates morphological masking and operations which is helpful for segmentation. The utilization of LP in fusion method suggested the medical image fragments into different sizes. Then the LP is utilized to fuse the four various decomposed layers. The developed model minimizes the

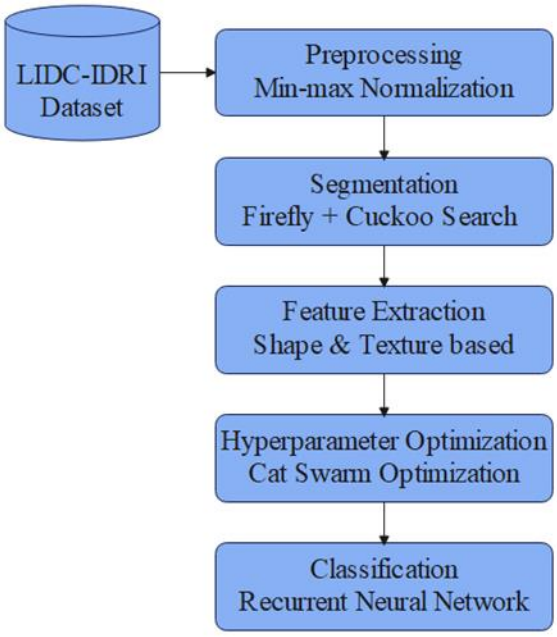

Figure. 1 Work flow of the proposed methodology

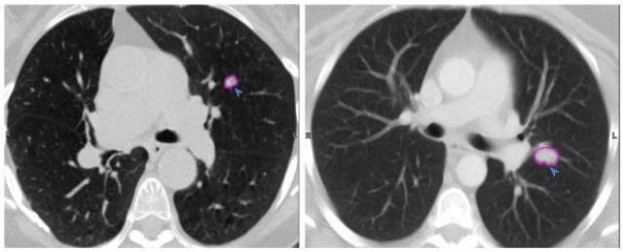

Figure. 2 Sample images for the LIDC-IDRI dataset

computational time which enhance the performance accuracy. However, the drawback of this developed model is computational time and it only applied on a single dataset.

3. Proposed method

The workflow of the proposed method is represented in Fig. 1. This proposed method is utilized for Nodule segmentation of lung CT image for medical applications using LIDC-IDRI dataset. Fig. 1 represents six different methods which include dataset, preprocessing, segmentation, feature extraction, hyperparameter optimization and classification.

3.1 Dataset

In this manuscript, the lung image database consortium and image database resource initiative (LIDC-IDRI) dataset [21] are used, which is a freely accessible dataset for CT lung images. This dataset is produced for the improvement in CAD for estimating lung nodule recognition, quantification and classification. The dataset contains 1018 diagnostics and 1010 individuals screening thoracic CT images with the elucidated lesions. All thoracic CT scans are under the two-stage annotation procedure generated by the four certified radiologists. These datasets are preprocessed by using min-max normalization method. Fig. 2 shows the sample images for the LIDC-IDRI dataset.

3.2 Preprocessing

Data preprocessing is the process of converting the raw data into a desired format, the dataset from several resources may consist of incomplete data. So, for further analysis, this data requires to be filtered and normalized [22]. Data normalization is the process of preprocessing the input data. The LIDC-IDRI dataset is standardized using min-max normalization methods. The highest score of the feature is transformed into 1, the smallest score of the feature is transformed into 0 and other values of the feature are transformed into an integer between 0 and 1. The mathematical representation of min-max normalization is shown in Eq. (1).

$$v' = \frac{v - min_A}{max_A - min_A}\left(new_{max_A} - new_{min_A}\right) + new_{min_A} \quad (1)$$

Where, v' is the respective min-max normalization value of the attribute, v is the primary value of the attribute, max_A is the highest score and min_A is the smallest score of the feature.

3.3 Lung nodule segmentation using MRF based firefly and cuckoo search algorithm

The input CT image C_m is considered as input of lung nodule segmentation where the segmentation process is recognized using markov random field (MRF) based FA and CS. The MRF weight is trained by the combination FA and CS algorithms and it provides a precise segmentation region for lung nodule classification. The benefit of using the MRF segmentation model offers a better-segmented outcome based on energy function, Bayesian framework, and spatial and intensity distribution scheme. In this paper, the lung nodule segmentation is performed before classifying the lung nodule since the segmentation process enhances the effectiveness of the classification outcome. Fig. 3 shows the segmentation result for the lung nodule.

Based on MRF, the affected region is segmented by using Eq. (2),

$$T(N = n|B = b) = A' \exp[-\beta(n, b)] \quad (2)$$

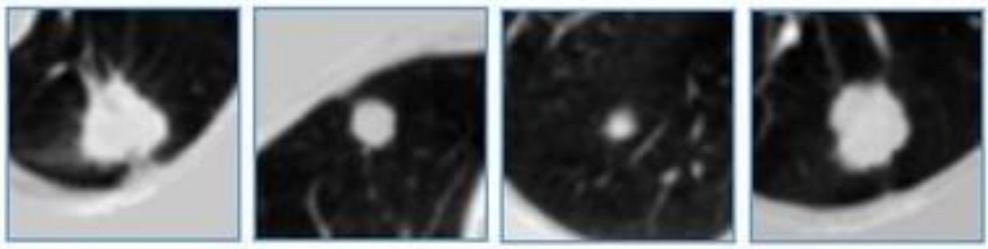

Figure. 3 Segmentation result for the lung nodule

Where, A' is the constant value and $\beta(n,b)$ is calculated as Eq. (3),

$$\beta(n,b) = \sum_{o=1}^{U}\sum_{r\in\varphi_o}\left[y(b_r,n) + \vartheta\sum_{d=\varpi,d\neq r}J_2(n_r,n_d)\right] \quad (3)$$

Thus, the highest value of probability function $T(N=n|B=b)$ is similar to the smallest value of energy function $\beta(n,b)$. The segmentation result n^* is discovered by Eq. (4),

$$n^* = arg_{n=\varphi_N}\min\{\beta(n,b)\} \quad (4)$$

The energy function expression $\beta(n,b)$ is calculated as Eq. (5),

$$\beta(n,b) = \sum_{o=1}^{U}\alpha(o)\sum_{r\in\varphi_o}\left[y(b_r,n) + \vartheta\sum_{d=\varpi,d\neq r}J_2(n_r,n_d)\right] = \sum_{o=1}^{U}\alpha(o)W(o) \quad (5)$$

Where, the $W(o)$ indicates the energy and $\alpha(o)$ specifies the weighting metric of o^{th} region. The weighting metric $\alpha(o)$ is trained by the combination of FA and CS algorithm. Hence, the segmented nodule region is demonstrated as n.

3.3.1. FACA model for the optimal tuning of weight metric

This section describes the FACA model for training the weight of MRF. The FACA model is designed by the integration of firefly algorithm (FA) and the cuckoo search algorithm (CSA). The FA is a swarm-based metaheuristic algorithm and it mimics the behavior of fireflies to get optimal solutions and it works well in the behavior of fireflies. The firefly's mathematical method is fully based on the following regulations:

1. The fireflies are attracted to each other.
2. The attraction between the fireflies is inversely proportional to the distance between them.
3. The attraction level is described by the brightness level. The low-brightness fireflies are to be attracted by the high brightness fireflies. The fireflies move randomly, because of their equal brightness level, so it fully depends on the objective function.

The attraction level between fireflies is inversely proportional to the distance, the level of attraction (β) at the distance (r) is presented in Eq. (6) as;

$$\beta(r) = \frac{\beta_0}{(1+\gamma\times r^2)} \quad (6)$$

Where, β_0 is the attractiveness level and γ is the coefficient of light absorption at $\gamma = 0$. r is the cartesian distance between two fireflies.

The CSA is a bio-inspired metaheuristic optimization algorithm that is modeled based on mimicking characteristics of cuckoo birds. This bird makes fantastic sounds and has an excellent reproduction strategy. To establish reproduction, the cuckoo laid their eggs in others nests by draining others' eggs from the nest. The CSA has three types of brood parasitism, which are collaborative breeding, nest acquisition as well and intraspecific brood parasitism. The CSA basic rules are explained as follows. Every cuckoo bird brings one egg, while selecting the nest as well as the best nest is used for the next generation. The nest has good eggs that are called the local solution which is used for reproduction. $Levy$ an air tips which is named as flights and are processed to find the result to good globally which is formulated in Eq. (7),

$$X_i^{t+1} = X_i + \alpha \oplus Levy(\lambda) \quad (7)$$

Where, X_i^{t+1} represents the output, X_i represents the present status and α represents the step or transition size.

3.4 Feature extraction

After the segmentation process, the features are extracted using shape and texture-based feature extraction. By using this technique, the LIDC-IDRI dataset is much more informative.

3.4.1. Shape-based feature extraction

The shape-based feature extraction is primarily performed to the shape properties like region, moment, and boundary in the image. Such extraction simplifies the transmission, identification, recognition and comparison of the shape. Shape-based features must be robust to conversion, scaling, and rotation. In this concern, there is no arithmetical transformation is implicated in shape features. The image has three values in every pixel and in the shape feature extraction the color image is converted into the greyscale images. For this purpose, the Eq. (8) is introduced by craig as shown below:

$$I_g = \left[I_r I_g I_b\right] \times 0.29890.5870.114 \quad (8)$$

Where, I_g is the grey-level image, $I_r I_g I_b$ is the component of the color. Neurotrophic clustering is used to divide pixels with the nearest value and avoiding pixels from greyscale images.

3.4.2. Texture-based feature extraction

The texture-based feature extraction is based on extracting several features from a grey level co-occurrence matrix (GLCM) model. This GLCM is an effective and robust methodology that analyses images and it is represented as a combined 2D matrix between pixels and pairs with distance d and direction θ. To classify the texture features, 14 features are extracted from GLCM method. The texture-based feature extraction using GLCM is presented in the following steps:

1. The colored image is converted into a greyscale image.
2. Input image is filtered using 5×5 matrix of Gaussian filter.
3. The filtered image is separated in 4×4 matrix blocks.
4. The GLCM evaluates every block of energy, contrast, mean value, standard deviation and homogeneity. The evaluation is done with four directions of these features namely vertical, horizontal, and diagonal direction.
5. These extracted features are stored in the database.

3.5 Hyperparameter optimization

In this proposed method, the cat swarm optimization (CSO) algorithm [23] is used for optimizing the nodule segmentation. In this CSO, first, select how many cats to use and then implement the cats within the CSO model to resolve the optimization issues. The behaviors of the cat are classified into two different manners such as seeking mode and tracing mode. The CSO obtained better performance at the final output till it reached the iterations at the end. The hyperparameter has some ranges like decay factor [0 to 1], maximum epochs [50 to 500], learning rate [0 to 0.1] and momentum [0.5 to 0.9]. These are the hyperparameter ranges by using CSO, it will provide best value from these ranges and it is called the best hyperparameter set. By using the hyperparameter tuning for optimization which improves the prediction accuracy of this model. The hyperparameter tuning is important for controlling the behavior of the model. The optimal hyperparameter leads to better efficiency, and quick convergence and provides better results.

3.5.1. Seeking mode

The seeking mode is employed for processing the cat and it moves carefully and slowly. In the seeking mode, there are four necessary elements seeking memory pool (SMP), seeking a range of selected dimension (SRD), counts of dimensions to change (CDC), and self position consideration (SPC). The SMP is employed to decide measurements in seeking memory of individual cats, it represents the desired position of the cat. From the memory pool, the cat can select a position by using corresponding rules. The SRD is specified as the selected dimension of the mutative ratio and it is a condition for transforming the size measurement. In seeking mode, the measurement is preferred for mutate, the comparison among the existing score and the new score will be within the specified limit. The CDC exhibits the value of how many size measurements will be differed. In seeking mode, these factors play a significant role. The moving positions of the candidate in the SPC determine the cat standing areas. The SPC score is considered as Boolean value either true or false. The procedure of seeking mode is represented in the below steps.

1. Consider the current position in j number of copies for cat_k ,where $j = SMP$ if the SPC score is considered as true, $j = SMP - 1$ if SPC score is considered as false means, then considered the present position as an individual candidate solution.
2. For all the copies based on CDC, minimize or maximize the SRD process of the present value and replace the existing value as Eq. (9),

$$Xjd_{new} = (1 + rand \times SRD) \times Xjd_{old} \quad (9)$$

Where, Xjd_{new}, Xjd_{old} is the updated position and the existing position of the cat_k respectively. d represents the dimensions, j illustrates the total amount of cat and $rand$ is the random number range of [0,1].

3. Estimate the fitness value of the overall candidate.
4. If the entire fitness value is not accurately the same, evaluate the selecting possibility of all the candidates using the below formula or else fix the selecting possibility of all the candidates to be 1.
5. Selecting the random position moving from the candidate point and replacing the position of cat_k is shown in Eq. (10),

$$P_i = \frac{|FS_i - FS_b|}{FS_{max} - FS_{min}} \quad (10)$$

If the goal of the fitness score is to reduce, then $FS_b = FS_{max}$, or else $FS_b = FS_{min}$, where the FS_{min} and FS_{max} represents the smallest and highest candidate fitness score correspondingly.

6. Classify and select the candidates by P_i and replace the position of cat_k.

3.5.2. Tracing mode

The tracing mode is the process of tracing some targets. The cat is once within the trace mode then it moves each dimension to its respective speed. The procedure of tracing mode is represented in the following steps.

1. Update the velocity of all dimension $(v_{k,d})$ corresponding to the Eq. (11),

$$V_{k,d}(\mathrm{t}+1) = V_{k,d}(\mathrm{t}) + r_1 c_1 \left(X_{best,d}(\mathrm{t}) - X_{k,d}(t)\right) \quad (11)$$

Where, $V_{k,d}(t+1)$ and $V_{k,d}$ is the velocity of the cat_k on the dimension d at time $t+1$ and t respectively, r_1 and c_1 illustrates the random score in the range of [0,1] and fixed value respectively. $X_{k,d}(t)$ is the coordination of the cat_k on dimension d at time $t+1$, $X_{best,d}(t)$ is the coordination with the better result on dimension d.

2. Verify that the velocity of each cat is adjacent to the highest speed. In that instance, if the updated speed score is in the high range, set the updated score equivalent to the restriction.
3. Update the cat position by inserting the updated speed and gain the entire cat position as Eq. (12),

$$x_{k,d}(\mathrm{t}+1) = x_{k,d}(\mathrm{t}) + V_{k,d}(t+1) \quad (12)$$

Where, $V_{k,d}(t+1)$ illustrates the velocity of the cat_k on the dth dimension at time $t+1$, $X_{k,d}(t+1)$ and $x_{k,d}(t)$ illustrates the coordination of cat_k on the dth dimension at time $t+1$ and t respectively. Then evaluate the fitness score of the updated cat position of the entire cat. At the time, tracing mode and searching mode are merged by employing a mixture ratio. Most of the time cats are spent resting, remaining time they move slowly and carefully. Once the cat is spending a lot of time in searching mode, it concludes that the mixture ratio is a minimum value. The cat swarm optimization is used for the hyperparameter tuning and it is further fed to the classifier.

3.6 Classification

After the hyperparameter optimization, recurrent neural network (RNN) is used to classify the lung nodules. The RNN is one category of neural networks that produces a direct graph by using a sequence of data [24]. RNN decides the present layer output by involving all other existing calculations. It differs from a classic neural network, in which all the input values are similar to each other. The following steps represent the training flow of RNN in classification.

Step 1: The network is supplied with individual time of input steps.

Step 2: Current input and earlier state are used for evaluating the current state.

Step 3: For the upcoming time steps, the current state ht is transferred to the $ht-1$.

Step 4: At all times steps can be built based on the problems. The instruction is merged from the earlier state.

Step 5: After completing all the time steps, the last current state is employed by the outputs.

Step 6: For updating the weights, the fault is back-propagated to the network. Therefore, RNN is trained.

In RNN every input is transferred to the next layer and the output of every layer fully depends on the previous layer. So, it is called a recurrent neural network and it accomplishes the same function for each component. The function of RNN with time-series data efficiently and the output of RNN obtains the best result and determines the previous information. The RNN combines the output and forgets gate into a specific update gate up_d, in which the linear interpolation method is used to obtain a better result. Assume that the $e_d \leftarrow Fr_{k^*}$ is the input feature of dimension d, H_{d-1} represents the hidden previous state. The Eqs. (13) and (14) represents the

output of the update gate up_d and the reset gate rs_d.

$$up_d = acv(WF^{eup} e_d + WF^{Hup} H_{d-1}) \quad (13)$$

$$rs_d = acv(WF^{ers} e_d + WF^{Hrs} H_{d-1}) \quad (14)$$

Where, acv represents the activation function, in general activation function is a logistic sigmoid function. $WF^d = WF^{eup}, WF^{ers}, WF^{Hup}, WF^{Hrs}$ is denoted by the weight function which is tuned by the training algorithm to decrease the error variation among the actual and forecasted outputs. The state of the candidate of the hidden unit is represented in Eq. (15).

$$\overline{H_d} = tan(WF^{eH} e_d + WF^{HH}(H_{d-1} \otimes rs_d)) \quad (15)$$

Where, $\otimes$ is the element-wise multiplication. The linear interpolation among candidate state $\overline{H_d}$ and H_{d-1} and additionally hidden activation function in the term d is represented as the H_d of the RNN is illustrated in Eq. (16).

$$H_d = (1 - up_d) \otimes \overline{H_d} + up_d \otimes H_{d-1} H_d = (1 - up_d) \otimes \overline{H_d} + up_d \otimes H_{d-1} \quad (16)$$

Where, H_{d-1} represents the hidden previous state and $\otimes$ is the element wise multiplication. In neural network, all output and input values are independent whereas, in the RNN remember the data in the hidden layer and it was completed in a previous hidden layer and permit the remembered data as input to the next layer so that only it can perform operations on data. This procedure is continuously repeated until it obtains the preferred output which is formulated in Eq. (17), (18) and (19),

$$h_t = f(h_{t-1}, x_t) \quad (17)$$

$$h_1 = \tan h\ (W_{hh} h_{t-1} + W_{xh} X_t) \quad (18)$$

$$y_t = W_{hv} h_t \quad (19)$$

This RNN takes the sequence of inputs from x_0 and then it outputs the sequence is h_0 which combines with the x_1 It is the input for the next process. The x_1 and h_0 is the input for the next process similarly, h_1 from the next process is the input with x_2 for the next step.

4. Result

The loss function plays a significant role in the training of neural networks. The loss function is utilized to assess the instability among the actual and the predicted values by using the model and it can be backpropagated with the last layer to improve the optimization density. Segmentation of CT image is necessary to convert into the background and foreground classification issues. When the testcase is in the positive section and the classifier accurately predicts it is a positive testcase, it is defined as true positive (TP). When a positive testcase is incorrectly predicted to be negative test case, it is defined as false positive (FP). Likewise, when a negative testcase is accurately predicted it is a negative testcase, it is defined as true negative (TN). When positive testcase is incorrectly predicted to be negative testcase, it is defined as false negative (FN). In the following formula, the actual image is represented as $T \in [0,1]^{m \times n}$ and the predicted value is represented as $P \in [0,1]^{m \times n}$, where n is every pixel value space in image N. Table 1 shows the performance metrices for the segmentation and classification.

Table 1. Performance metrices for segmentation and classification

Segmentation Performance Metrices	
Parameters	**Equation**
Accuracy	$\frac{TP + TN}{TP + FP + TN + FN}$
Sensitivity	$\frac{TP}{TP + FN}$
Dice Coefficient (DC)	$\frac{2 \times TP}{(TP + FP) + (TP + FN)}$
Mean Intersection Over Union (MIOU)	$\frac{1}{k+1} \sum_{i=0}^{k} \frac{TP}{FN + FP + TP}$
Classification Performance Metrices	
Parameters	**Equation**
Accuracy	$\frac{TP + TN}{TP + FP + TN + FN}$
Sensitivity	$\frac{TP}{TP + FN}$
Specificity	$\frac{TN}{TN + FP}$
F1-score	$\frac{2TP}{2TP + FN + FP}$

Where i and j is the actual and the predicted value, p_{ii} and p_{ij} is the actual number and number of j predicted from the actual value i respectively. $k + 1$ is the number of classes. The TP, TN, FP and FN represent the true positive, true negative, false positive and false negative correspondingly.

4.1 Quantitative analysis

This section shows the quantitative analysis of the RNN model without augmentation in dice coefficient (DC) loss, mean intersection over union (MIOU),

Table 2. Represents the segmentation result with state of art methods

Methods	Dice (%)	Accuracy (%)	Sensitivity (%)	MIOU (%)
Otsu's Threshold	91.76	92.88	92.18	91.46
K-means algorithm	93.79	93.96	92.34	92.64
Region growing	94.95	95.05	95.70	94.89
FA+CSA with proposed MRF	96.28	98.65	95.86	96.06

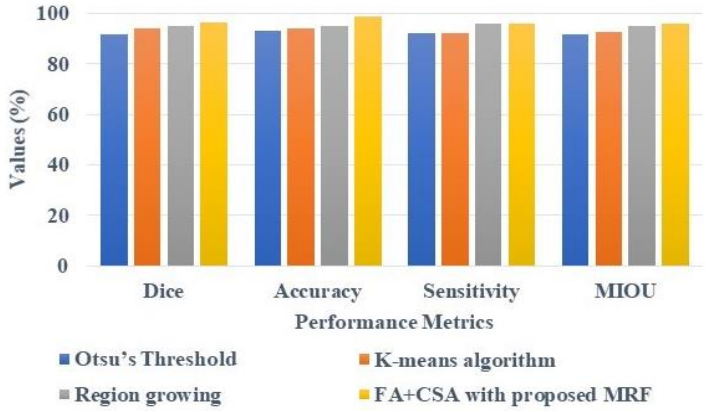

Figure. 4 Represents the segmentation result with state of art methods

Table 3. Represents the segmentation result with different optimization with MRF

Methods	Dice (%)	Accuracy (%)	Sensitivity (%)	MIOU (%)
PSO	87.25	91.79	88.27	88.79
GWO	91.74	93.67	90.48	92.34
ACO	92.56	96.09	93.93	94.12
FA+CSA with proposed MRF	96.28	98.65	95.86	96.06

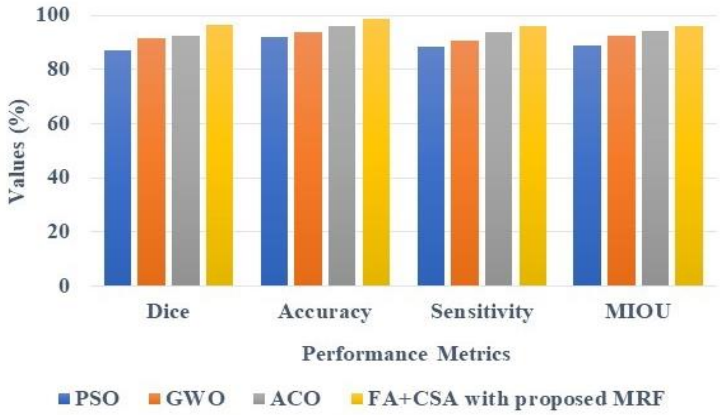

Figure. 5 Represents the segmentation result with different optimizations with MRF

sensitivity and accuracy are shown in Tables 1 and 2 respectively. Table 1 presents the quantitative analysis of several classifier by employing the LIDC-IDRI dataset. Table 2 presented the quantitative analysis of several optimization by employing the LIDC-IDRI dataset.

Table 2 and Fig. 4 shows the performance measure of various optimization for LIDC-IDRI dataset. The DC, MIOU, specificity and accuracy of Otsu's threshold, K-means algorithm, region growth are measured and matched with the proposed Firefly and cuckoo search algorithm with MRF model. The obtained result shows that the proposed FA+CSA with MRF model achieves better results by using performance metrics like DC, accuracy, sensitivity, and MIOU values of about 96.28%, 98.65%, 95.86%, and 96.06% respectively while comparing to another optimization.

Table 3 and Fig. 5 shows the performance measure of various classification for LIDC-IDRI dataset. The DC, MIOU, specificity and accuracy of the particle swarm optimization (PSO), grey wolf

Table 4. Represents the classification result with state of art methods

Methods	Accuracy (%)	Sensitivity (%)	Specificity (%)	F1-score (%)
FCN	83.13	82.62	82.46	82.75
CNN	85.54	84.43	84.39	85.21
GAN	87.48	87.17	87.30	87.28
Leenet	88.97	88.63	88.71	88.54
CSO with proposed RNN	90.28	91.12	90.18	90.05

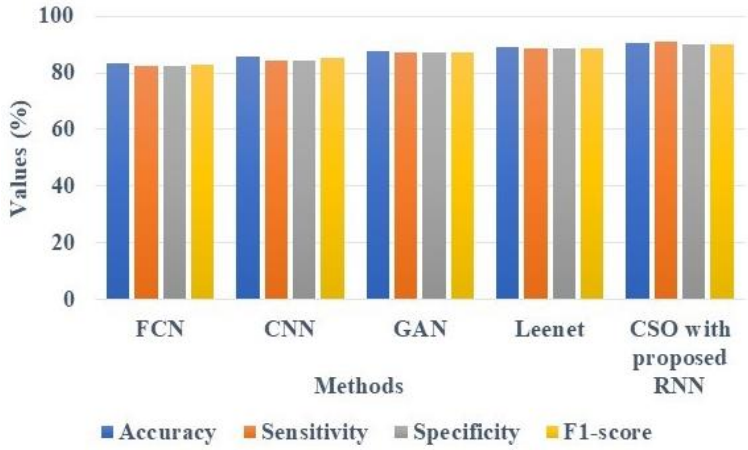

Figure. 6 Represents the classification result with state of art methods

Table 5. Represents the classification result for different optimization algorithm with MRF.

Methods	Accuracy (%)	Sensitivity (%)	Specificity (%)	F1-score (%)
SGD	84.71	84.14	84.26	89.51
GWO	86.34	86.21	86.32	86.16
SSA	87.96	87.43	87.54	87.71
ACO	89.39	89.26	89.12	89.09
CSO with proposed RNN	90.28	91.12	90.18	90.05

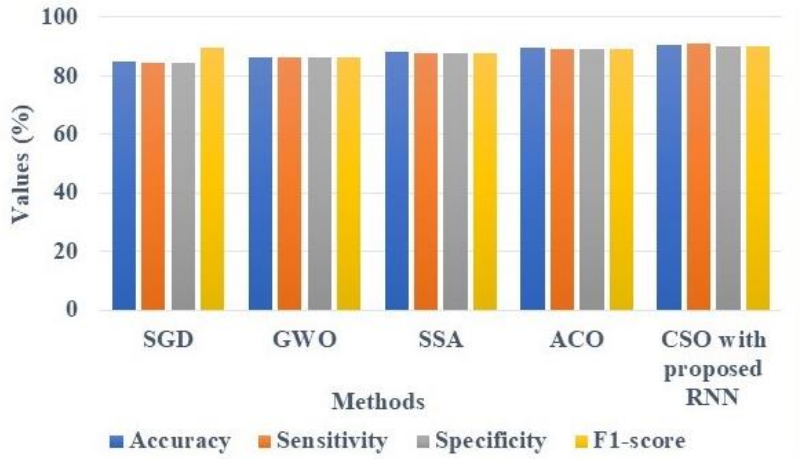

Figure. 7 Represents the classification result for different optimization algorithms with MRF

optimization (GWO), ant colony optimization (ACO) are measured and matched this proposed FA+CSA with MRF model. The obtained result shows that the proposed FA+CSA with MRF model achieves better results by using performance metrics like dice, accuracy, sensitivity and MIOU values about 96.28%, 98.65%, 95.86% and 96.06% respectively while comparing to various classification algorithms.

Table 4 and Fig. 6 shows the performance measure of various optimization for LIDC-IDRI dataset. The accuracy, sensitivity, specificity and F1-score of the FCN, CNN, GAN, LeeNet are measured

Table 6. Comparative analysis of proposed method with various other methods

Author	Dataset	Accuracy (%)	Sensitivity (%)
Usman and Shin [15]	LIDC-IDRI	N/A	90.84
Inayatul Haq [19]		84.8	79.5
Imran Nazir [20]		N/A	89
Proposed Method		90.28	91.12

and matched with this proposed cat swarm optimization (CSO) based recurrent neural network (RNN) model. The obtained result shows that the proposed CSO model achieves better results by using performance metrics like accuracy, sensitivity, specificity and F1-score values of about 90.28%, 91.12%, 90.18% and 90.05% respectively while comparing to various optimization algorithm.

Table 5 and Fig. 7 shows the performance measure of various classification methods. The accuracy, sensitivity, specificity and F1-score of the stochastic gradient descent (SGD), grey wolf optimization (GWO), salp swarm optimization algorithm (SSA) and ant colony optimization (ACO) are measured and matched with this proposed cat swarm optimization (CSO) based recurrent neural network (RNN) model. The obtained result shows that the proposed CSO base RNN model achieves better results by using performance metrics like accuracy, sensitivity, specificity and F1-score values about 90.28%, 91.12%, 90.18% and 90.05% respectively while comparing to various classification algorithm.

4.2 Comparative analysis

This section demonstrates the comparative analysis of RNN classifier with performance metrics like Sensitivity and Accuracy as shown in Table 6. Existing research such as [15, 19, 20] are used for evaluating the ability of the proposed method. This proposed method is trained, tested, and verified by utilizing the LIDC-IDRI dataset for creating same environment. The accuracy and sensitivity were improved 90.28% and 91.12% respectively. The proposed CSO based RNN was evaluated for efficient classification using the RNN technique by overcoming overfitting problems and dataset classification.

5. Summary

Nodule segmentation in lung CT images is an important part of the analysis of lung images, which is also useful in the recognition of lung tumors. In this paper, the cat swarm optimization (CSO) based recurrent neural network (RNN) model is proposed using the LIDC-IDRI dataset for lung nodule segmentation. The lung image database consortium and image database resource initiative (LIDC-IDRI) dataset is utilized which is publicly available for lung CT images. This dataset contains 1018 diagnostics and 1010 individuals screening thoracic CT images for lung cancer with the elucidated lesions. The input CT image is considered as input of lung nodule segmentation where the segmentation process is recognized using the firefly algorithm and the cuckoo search algorithm. The CT image features are extracted using shape and texture-based feature extraction which generate lung data more informative. From the result, the proposed CSO based RNN model delivers performance metrics like dice coefficient (DC) loss and accuracy values about 96.28% and 90.28% respectively which ensures accurate nodule segmentation in lung CT images. The future work is to improve the segmentation performance for better lung nodule segmentation.

Notations

Notation	Description
v'	Min-max normalization value
v	Primary value of the attribute
max_A	Maximum score of the feature
min_A	Minimum score of the feature
A'	Constant value
$\beta(n,b)$	Energy function
n^*	Segmentation result
$W(o)$	Energy of o^{th} region
$\alpha(o)$	Weighting metric of o^{th} region
$\beta(r)$	Level of attraction (β) at the distance (r)
β_0	Attractiveness level
γ	Coefficient of light absorption
r	Cartesian distance between two fireflies
X_i^{t+1}	Levy output
X_i	Present status
α	Step or transition size
I_g	Grey-level image
$I_r I_g I_b$	Component of the color
Xjd_{new}	Updated position of the cat_k
Xjd_{old}	Existing position of the cat_k
d	Dimensions of cat
j	Total amount of cat
$rand$	Random number range of [0,1]

P_i	Position of cat_k
FS_{min}	Smallest candidate fitness score
FS_{max}	Highest candidate fitness score
$V_{k,d}(t+1)$	Velocity of the cat_k on dimension d at time $(t+1)$
$V_{k,d}(t)$	Velocity of the cat_k on dimension d at time (t)
r_1	Random score in the range of [0,1]
c_1	Fixed value
$X_{k,d}(t+1)$	Coordination of the cat_k on dimension d at time $(t+1)$
$X_{k,d}(t)$	Coordination of the cat_k on dimension d at time (t)
$X_{best,d}(t)$	Coordination with better result on dimension d at time (t)
acv	Activation function
WF^d	Weight function
$\otimes$	Element-wise multiplication
H_{d-1}	Hidden previous state
$k+1$	Number of classes
TP	True Positive
TN	True Negative
FP	False Positive
FN	False Negative

Conflicts of interest

The authors declare no conflict of interest.

Author contributions

For this research work all authors' have equally contributed in conceptualization, methodology, validation, resources, writing—original draft preparation, writing—review and editing.

References

[1] Z. Wu, Q. Zhou, and F. Wang, "Coarse-to-Fine Lung Nodule Segmentation in CT Images With Image Enhancement and Dual-Branch Network", *IEEE Access*, Vol. 9, pp. 7255-7262, 2021.

[2] M. Maqsood, S. Yasmin, I. Mehmood, M. Bukhari, and M. Kim, "An Efficient DA-Net Architecture for Lung Nodule Segmentation", *Mathematics*, Vol. 9, No. 13, p. 1457, 2021.

[3] R. Shetty and P. N. Sarappadi, "Self-Sequential Attention Layer based DenseNet for Thoracic Diseases Detection", *International Journal of Intelligent Engineering & Systems*, Vol. 14, No. 4, pp. 157-165, 2021, doi: 10.22266/ijies2021.0831.15.

[4] M. A. Khan, V. Rajinikanth, S. C. Satapathy, D. Taniar, J. R. Mohanty, U. Tariq, and R. Damaševičius, "VGG19 Network Assisted Joint Segmentation and Classification of Lung Nodules in CT Images", *Diagnostics*, Vol. 11, No. 12, p. 2208, 2021.

[5] C. S. R. Annavarapu, S. A. B. Parisapogu, N. V. Keetha, P. K. Donta, and G. Rajita, "A Bi-FPN-Based Encoder–Decoder Model for Lung Nodule Image Segmentation", *Diagnostics*, Vol. 13, No. 8, p. 1406, 2023.

[6] A. Bilal, M. Shafiq, F. Fang, M. Waqar, I. Ullah, Y. Y. Ghadi, H. Long, and R. Zeng, "IGWO-IVNet3: DL-Based Automatic Diagnosis of Lung Nodules Using an Improved Gray Wolf Optimization and InceptionNet-V3", *Sensors*, Vol. 22, No, 24, p. 9603, 2022.

[7] M. Ibrahim, M. Mahmoud, R. M. Albadawy, and H. Abdulkader, "Liver Multi-class Tumour Segmentation and Detection Based on Hyperion Pre-trained Models", *International Journal of Intelligent Engineering & Systems*, Vol. 15, No. 6, pp. 392-405, 2022, doi: 10.22266/ijies2022.1231.36.

[8] K. Sekeroglu, and Ö. M. Soysal, "Multi-Perspective Hierarchical Deep-Fusion Learning Framework for Lung Nodule Classification. Sensors", *Sensors*, Vol. 22, No. 22, p. 8949, 2022

[9] Y. Jalali, M. Fateh, M. Rezvani, V. Abolghasemi, and M. H. Anisi, "ResBCDU-Net: A Deep Learning Framework for Lung CT Image Segmentation", *Sensors*, Vol. 21, No. 1, p. 268, 2021.

[10] M. Savic, Y. Ma, G. Ramponi, W. Du, and Y. Peng, "Lung Nodule Segmentation with a Region-Based Fast Marching Method", *Sensors*, Vol. 21, No. 5, p. 1908, 2021.

[11] R. J. Suji, S. S. Bhadouria, J. Dhar, and W. W. Godfrey, "Optical flow methods for lung nodule segmentation on LIDC-IDRI images", *Journal of Digital Imaging*, Vol. 33, No. 5, pp. 1306-1324, 2020.

[12] Y. Faradhilla, A. Z. Arifin, N. Suciati, E. R. Astuti, R. Indraswari, and M. Widiasri, "Residual Fully Convolutional Network for Mandibular Canal Segmentation", *International Journal of Intelligent Engineering and Systems*, Vol. 14, No. 6, pp. 208-219, 2021, doi: 10.22266/ijies2021.1231.20.

[13] N. Zhang, J. Lin, B. Hui, B. Qiao, W. Yang, R. Shang, X. Wang, and J. Lei, "Lung nodule segmentation and recognition algorithm based on multiposition U-net", *Computational and Mathematical Methods in Medicine*, Vol. 2022, p. 5112867, 2022.

[14] X. Zhang, S. Kong, Y. Han, B. Xie, and C. Liu, "Lung Nodule CT Image Segmentation Model Based on Multiscale Dense Residual Neural Network", *Mathematics*, Vol. 11, No. 6, p. 1363,

2023.

[15] M. Usman and Y. G. Shin, "DEHA-Net: A Dual-Encoder-Based Hard Attention Network with an Adaptive ROI Mechanism for Lung Nodule Segmentation", *Sensors*, Vol. 23, No. 4, p. 1989, 2023.

[16] S. F. Banu, M. M. K. Sarker, M. A. Nasser, D. Puig, and H. A. Raswan, "AWEU-Net: An Attention-Aware Weight Excitation U-Net for Lung Nodule Segmentation", *Applied Sciences*, Vol. 11, No. 21, p. 10132, 2021.

[17] Z. Shi, Q. Hu, Y. Yue, Z. Wang, O. M. S. A. L. Othmani, and H. Li, "Automatic nodule segmentation method for CT images using aggregation-U-Net generative adversarial networks", *Sensing and Imaging*, Vol. 21, No. 1, p. 39, 2020.

[18] G. Singadkar, A. Mahajan, M. Thakur, and S. Talbar, "Deep deconvolutional residual network based automatic lung nodule segmentation", *Journal of Digital Imaging*, Vol. 33, No. 3, pp. 678-684, 2020.

[19] I. Haq, T. Mazhar, M. A. Malik, M. M. Kamal, I. Ullah, T. Kim, M. Hamdi, and H. Hamam, "Lung Nodules Localization and Report Analysis from Computerized Tomography (CT) Scan Using a Novel Machine Learning Approach", *Applied Sciences*, Vol. 12, No. 24, p. 12614, 2022.

[20] I. Nazir, I. U. Haq, M. M. Khan, M. B. Qureshi, H. Ullah, and S. Butt, "Efficient pre-processing and segmentation for lung cancer detection using fused CT images", *Electronics*, Vol. 11, No. 1, p. 34, 2021.

[21] Dataset link: https://wiki.cancerimagingarchive.net/display/Public/LIDC-IDRI.

[22] S. S. Mallela and S. K. Jonnalagadda, "Rainfall Prediction Based on Spatial Attention Layer: A Case Study Analysis", *International Journal of Intelligent Engineering & Systems*, Vol. 15, No. 3, pp. 49-58, 2022, doi: 10.22266/ijies2022.0630.05.

[23] T. Nagadurga, P. V. R. L. Narasimham, and V. S. Vakula, "Global Maximum Power Point Tracking of Solar Photovoltaic Strings under Partial Shading Conditions Using Cat Swarm Optimization Technique", *Sustainability*, Vol. 13, No. 19, p. 11106, 2021.

[24] V. Talasila, K. Madhubabu, M. C. Mahadasyam, N. J. Atchala, and L. S. Kande, "The Prediction of Diseases Using Rough Set Theory with Recurrent Neural Network in Big Data Analytics", *International Journal of Intelligent Engineering & Systems*, Vol. 13, No. 5, pp. 10-18, 2020, doi: 10.22266/ijies2020.1031.02.